HHS Public Access

Author manuscript

*Biochem J.* Author manuscript; available in PMC 2019 July 05.

Published in final edited form as:

*Biochem J.* ; 475(13): 2167–2177. doi:10.1042/BCJ20180317.

# Probing the specificity of CYP112 in bacterial gibberellin biosynthesis

**Raimund Nagel** and **Reuben J. Peters***

Roy J. Carver Department of Biochemistry, Biophysics and Molecular Biology, Iowa State University, Ames, IA, 50011, USA

## Abstract

Biosynthesis of the gibberellin A (GA) plant hormones evolved independently in plant-associated fungi and bacteria. While the relevant enzymes have distinct evolutionary origins, the pathways proceed via highly similar reactions. One particularly complex transformation involves combined demethylation and γ-lactone ring formation, catalyzed in bacteria by the cytochrome P450 CYP112 in three individual steps, which involves large structural changes in the transition from substrate to product, with further divergence in the recently demonstrated use of two separate mechanistic routes. Here the substrate specificity of the isozyme from *Erwinia tracheiphila*, *Et*CYP112, was probed via UV-Vis spectral binding studies and activity assays with alternate substrates from the GA biosynthetic pathway. *Et*CYP112 tightly binds its native substrate $GA_{12}$ and the intermediates $GA_{15}$ and $GA_{24}$, as well as the methylated derivatives of $GA_{12}$ and $GA_{15}$. It however only poorly binds methylated $GA_{24}$, its $GA_9$ final product and the C-20 carboxylate side-product $GA_{25}$. These distinct affinities are consistent with the known reactivity of *Et*CYP112. However, while it binds to the immediately preceding pathway metabolite $GA_{12}$-aldehyde and even earlier oxygenated *ent*-kaurene precursors, *Et*CYP112 only reacts with $GA_{12}$-aldehyde, and not the earlier *ent*-kaurene derived metabolites. But even with $GA_{12}$-aldehyde conversion is limited to the first two steps and the final combined demethylation and γ-lactone ring forming reaction is not catalyzed. Thus, CYP112 has evolved specificity at the catalytic rather than substrate binding level to enable its role in GA biosynthesis.

## Introduction

Gibberellins (GAs) are essential hormones in plants, and certain plant-associated fungi and bacteria also have acquired the ability to produce GAs in order to manipulate their host plants (1). The bacterial gibberellin biosynthetic pathway was elucidated very recently (Figure 1)(2–4). The steps of the individual pathways are quite similar between plants, fungi and bacteria. Nevertheless, at the enzyme level it is evident from the low sequence identity that GA biosynthesis evolved separately in plants, fungi and bacteria (1–4). One hallmark

*To whom correspondence should be addressed: Reuben J. Peters, rjpeters@iastate.edu.

**Conflict of interest**

The authors declare that they have no conflicts of interest with the contents of this article.

**Author Contributions**

R.N. performed experiments and analyzed data; R.N. and R.J.P. conceived the experiments and wrote the manuscript.

transformation in GA biosynthesis is the conversion of 20-carbon GAs to the 19-carbon GAs, involving the combined loss of a methyl group and the formation of an intramolecular γ-lactone bridge. Plants mediate this complex multi-step reaction with 2-oxoglutarate dependent dioxygenases (2ODDs) termed GA 20-oxidase (GA20ox) and, although this transformation is mediated by cytochromes P450 (CYPs) in both fungi (CYP68B) and bacteria (CYP112), these two CYP sub-families share less than 15% sequence identity (1, 4). Moreover, while the relevant fungal CYP68B is membrane-bound, the bacterial CYP112 is soluble. Nonetheless, the chemical transformations catalyzed by the three individual enzymes appear to be identical, involving stepwise oxidation of C-20. Specifically hydroxylation of $GA_{12}$ at this position to form $GA_{15}$, followed by further oxidation to the aldehyde equivalent $GA_{24}$ and, finally, loss of C-20 as $CO_2$ with formation of the intramolecular γ-lactone bridge that yields $GA_9$ (5–9)(Figure 1). While the fungal enzyme does not react with the intermediates $GA_{15}$ or $GA_{24}$ and will only release them under sub-optimal conditions, the bacterial and plant enzymes release their intermediates more readily, and can use $GA_{15}$ and $GA_{24}$ as substrates to produce $GA_9$ (1, 4, 7, 9). Although all of these oxidases produce the C-20 carboxylate $GA_{25}$, this seems to be a side-product rather than intermediate, as it cannot be transformed to $GA_9$ by any of them.

The recently discovered bacterial CYP112 offers distinct advantages for study as, in contrast to the 2ODDs utilized by plants, CYPs change their spectral properties upon substrate binding. Unbound CYPs have a characteristic absorbance maximum around 420 nm, called the Soret-band, which shifts to around 390 nm upon binding of their substrates, and this spectral shift can be used to measure affinity (10). While the fungal CYP68B presumably undergoes a similar spectral shift, it is membrane bound, which significantly complicates expression and purification. Moreover, the fungal CYP68B does not release its reaction intermediates or exhibit reactivity with these, at least in the context of incubation with cultures of *Gibberella fujikuroi* to which these studies have been limited (11, 12). In contrast, the CYP112 from *Erwinia tracheiphila* (*Et*CYP112) can be readily recombinantly expressed in *Escherichia coli*, purified and assayed *in vitro*, with characterization of its reaction mechanism via $^{18}O$ labeling experiments recently reported (9). Specifically, *Et*CYP112 variably employs two diverging reaction mechanisms, with some significant difference in intermediates – i.e., either the open or closed (δ-lactone and lactol, respectively) forms of the intermediates $GA_{15}$ and $GA_{24}$ – that reconverge at a transient cyclic anhydride C-20 *geminal*-diol intermediate (Figure 1B). Thus, *Et*CYP112 is able to react with all potential intermediates, including those not utilized by either of the functionally equivalent enzymes from fungi or plants. In particular, as the fungal CYP68B has not been shown to react with any intermediate (11), while the plant GA20ox does not react with the closed lactone of $GA_{15}$ (7). This sparked interest as to the substrate specificity of *Et*CYP112, which was investigated here by UV-Vis monitored binding studies and *in vitro* activity assays with alternate substrates. The results demonstrate that, although *Et*CYP112 is able to bind multiple upstream metabolites, it only reacts with $GA_{12}$-aldehyde. However, the resulting transformation is limited to production of $GA_{15}$-aldehyde and $GA_{24}$-aldehyde.

## Experimental

### Cloning, Expression and Purification of EtCYP112 and EtFdR

Cloning of *Et*CYP112 and *Et*FdR was described previously (9). Plasmids containing either *Et*CYP112 or *Et*FdR were transformed into E. coli BL21-Star (Invitrogen) for expression. Starter cultures of 25 ml liquid NZY medium (10 g/L NaCl, 10 g /L casein, 5 g/L yeast extract, 1 g/L MgSO4 (anhydrous), pH 7.0), including 50 μg/mL carbenicillin, were inoculated with 3 individual colonies and incubated at 18 °C for 2 days with constant shaking at 200 rpm. Theses starter culture were used to inoculate 1 L of NZY with 50 μg/mL carbenicillin, which was kept at 18 °C with constant shaking at 200 rpm until an OD600 of 0.8 was reached. At this point the culture was induced with 1 mM IPTG and, for cultures expressing EtCYP112, 1 mM aminolevulinic acid, 1 mM riboflavin and 0.1 mM $FeCl_3$ were added. After 36 hours, the cells were harvested by centrifugation at 5000 x g for 20 min. The *Et*CYP112 cell pellet was re-suspended in 10 mL 25 mM 3-(N-morpholino)-2-hydroxypropanesulfonic acid (MOPSO), pH 7.2, 10% (v/v) glycerol), while the *Et*FdR cell pellet was re-suspended in 10 mL 50 mM phosphate, pH 7.5, 10% glycerol. Both cell suspensions were homogenized with an EmulsiFlex C-3 (Avestin, Canada). The lysate was centrifuged at 17,000 x g for 30 min. The cleared lysate was then added to 1 mL of Ni-NTA Agarose (Qiagen), with the corresponding buffer containing 1 M imidazole added to reach a final concentration of 20 mM imidazole. Columns were incubated with gentle shaking at 4 °C for 1 h. The column was washed with 5 mL buffer containing 20 mM imidazole and then 5 mL with 60 mM imidazole, before being eluted with the corresponding buffer with 250 mM imidazole. The eluted protein was then transferred to dialysis tubing with a molecular weight cutoff of 15 kDa and dialyzed 3 times against 1L of 10 mM MOPSO, pH 7.2, 5% (v/v) glycerol in the case of *Et*CYP112 when used for spectral binding studies or 25 mM phosphate, pH 7.5, 10% glycerol in the case of EtFdR, as well as EtCYP112 when used for enzymatic activity assays. The resulting enzymes were either used fresh or stored at −80 °C after flash freezing by brief immersion in liquid nitrogen of 0.5 mL aliquots in 1.5 mL Eppendorf tubes. Only fractions with ≥95% purity, as assessed by SDS-PAGE analysis, were used. The concentration of *Et*CYP112 was measured by optical absorbance at 280 nm, using the calculated extinction coefficient of 43,555 $M^{-1}$ $cm^{-1}$.

### Enzyme assays

Enzyme assays under regular atmosphere or $^{18}O_2$ were performed as described previously (9). Briefly, 0.01 mL each of purified *Et*CYP112, spinach ferredoxin (Sigma-Aldrich), and *Et*FdR (all at 1 mg/mL in 25 mM phosphate, pH 7.5, 10% glycerol) were diluted with 1.5 mL of 25 mM phosphate, pH 7.5, 10% glycerol in 4 mL clear glass vials, and 20 μM of the specified substrate and 60 μM NADPH were added. The vial was sealed with a Teflon-septum cap and incubated for 12 h at 25 °C. For $^{18}O_2$ labeling experiments these vials were first flushed with nitrogen for 5 min, then 0.05 mL each of purified *Et*CYP112, spinach ferredoxin (Sigma-Aldrich), and *Et*FdR (all at 1 mg/mL in 25 mM phosphate, pH 7.5, 10% glycerol), and 1.7 mL of 25 mM phosphate, pH 7.5, 10% glycerol were added using a syringe. $^{18}O_2$ (Sigma-Aldrich, 97% labeled; max loaded pressure less than 2.4 bar) was added from the gas cylinder via a needle through the septum until the pressure equilibrated between the tank and the vial. The reaction was started by the addition of substrate to a final

concentration of 40 μM. Assays from $^{18}O_2$ labeling experiments were analyzed with an Agilent 6540 GC coupled to a Waters GCT Premier mass spectrometer and a 3900 Saturn GC coupled to a 2100T ion trap mass spectrometer (Varian, Palo Alto, CA, USA), enzyme assays under regular atmosphere were only analyzed with the 3900 Saturn GC coupled to a 2100T ion trap mass spectrometer. Separation was achieved over a DB-5MS column (30 m, 250 μm, 0.25 μm) with a previously described temperature gradient (3). For further conversion of the $GA_{12}$-aldehyde products, two-thirds of the organic solvent extract from the primary *in vitro* enzyme assay were split off and, after evaporation, dissolved in 300 μL of methanol:DMSO (1:1, v/v) without methylation. This material fed to the GA operon SDR from *E. tracheiphila* (*Et*SDR), much as previously described (2). Briefly, this was done via whole-cell feeding for three days to a recombinant culture of *E. coli* expressing *Et*SDR, with subsequent extraction and analysis by GC-MS.

### UV-Vis spectroscopy

Purified *Et*CYP112 in 10 mM MOPSO, pH 7.2, 5% (v/v) glycerol was diluted in the same buffer so that absorbance at 419 nm was 0.6 – 0.7 and spectra from 300 to 700 nm were collected on a Cary 50 UV-VIS spectrometer (Varian) at a scan rate of 60 nm per minute. Substrates were added stepwise from a stock solution of 0.1 or 1 mg/mL dissolved in methanol. Methanol was added to *Et*CYP112 as a control for spectral shifts originating from the solvent alone, although no changes in the UV-Vis spectrum were observed with up to 8% methanol (v/v). $K_d$ for individual binding curves were calculated using plots of the added substrate concentration versus the induced spectral shifts, the curve was then fitted using the model for tight binding ligands with the following formula.

$$A_{obs} = \left(\frac{A_{max}}{2 * E_t}\right) * (\mathrm{S} + E_t + K_d) - \sqrt{(S + E_t + K_d)^2 - (4 * S * E_t)}$$

The mean and standard error were calculated from three individual experiments and reported in Table 1.

## Results

The previously described N-terminal His-tagged *Et*CYP112 construct was found to be expressed to about 15 mg/ml in *E. coli* and easily purified by nickel affinity chromatography. UV-Vis spectral analysis found that the eluted preparation exhibited a Soret-band peak at 424 nm. Following dialysis, the substrate-free enzyme showed a more characteristic Soret-band maximum at 419 nm. Upon reduction and binding of carbon monoxide, purified *Et*CYP112 also exhibited the eponymous absorption peak at 450 nm (Supplemental Figure S1).

Upon addition of substrate or intermediates to purified *Et*CYP112, typical Type I binding spectra were observed. These are characterized by an almost complete shift of the Soret-band peak to 391 nm, as well as decreased α-band absorption at 570 nm. Given the evident high-affinity of *Et*CYP112 for these, their $K_d$ values were calculated from Soret-band shift data using the equation that applies to such tight-binding ligands (13). $K_d$ values for $GA_{12}$,

$GA_{15}$ (open lactone, added from a stock with 1 M KOH), $GA_{15}$ (closed δ-lactone) and $GA_{24}$ were calculated to be 2.6, 0.11, 0.6 and 0.3 μM respectively (Figures 2, S2 and Table 1). By contrast, the $GA_{25}$ side-product and the $GA_9$ final product only shift the Soret-band from 419 to 391 nm about 10–20% or 5% respectively, without any decrease of the α-band.

Previously, to elucidate the mechanism of CYP112 the carboxylates at C-7 and C-19 were methylated and the resulting compounds tested as substrates. While $MeGA_{12}$ and $MeGA_{15}$ (δ-lactone form) are converted by *Et*CYP112 to $GA_9$, $MeGA_{24}$ was not (9). Binding of these methylated GAs also was investigated here by UV-Vis spectral analysis (Table 1, Figures 3 and S3). Methylation of $GA_{12}$ ($MeGA_{12}$) reduced its affinity for *Et*CYP112, with a 5-fold higher $K_d$ observed than that measured for free $GA_{12}$. By contrast, $MeGA_{15}$ (closed δ-lactone) is bound about 6-fold more tightly by *Et*CYP112 than the analogous form of free $GA_{15}$, and its $K_d$ is more similar to the open form of $GA_{15}$. $MeGA_{24}$ on the other hand only induces a partial shift of the Soret-band, the binding curve could not be fit to the model for tight binding ligands, and there was no decrease in the absorption of the α-band.

Given the ability of *Et*CYP112 to act upon C-7 methyl ester derivatives, it seemed possible that it further might exhibit activity with the immediate precursor to $GA_{12}$ – $GA_{12}$-aldehyde – in which C-7 is an aldehyde rather than a carboxylate. Indeed, $GA_{12}$-aldehyde was found to be tightly bound by *Et*CYP112 in UV-Vis spectral studies, with a $K_d$ of 2.0 μM (Table 1 and Figures 3 and S3). When fed to the previously reported reconstituted enzymatic system, $GA_{12}$-aldehyde is transformed into two products, although conversion was not complete even in the presence of a 10-fold excess of NADPH (Figure 4). The two products exhibited molecular ions with 30 mass units less than those of one of the corresponding C-7 carboxylate containing GAs, consistent with the expected mass difference between an aldehyde and a (methylated) acid function (note that all of the compounds examined here were methylated for analysis by GC-MS)(Figure 5). Based on the ability of the short-chain alcohol dehydrogenase/reductase (SDR) found in the bacterial GA biosynthetic operon to convert $GA_{12}$-aldehyde to $GA_{12}$ (2–4), the observed products were incubated with *E. coli* expressing this SDR from *E. tracheiphila* (*Et*SDR). This led to conversion of one product to $GA_{24}$, indicating that this was $GA_{24}$-aldehyde. These had very similar retention times (Figure 4). Another product exhibited a similarly close retention time to $GA_{15}$, and has a very similar mass fragmentation pattern to $GA_{15}$ as well, suggesting that it is $GA_{15}$-aldehyde. This tentative assignment was further supported by $^{18}O$ labeling experiments, as the mass of the putative $GA_{15}$-aldehyde was increased by 2 mass units, while the mass of $GA_{24}$-aldehyde was increased by 2 mass units (about 30%) or 4 mass units (about 66%) (Figure 5). This labeling pattern is similar to that previously reported for the production of $GA_{24}$ from $GA_{12}$ (9, 13). The inability of *Et*SDR to convert the putative $GA_{15}$-aldehyde to the corresponding C-7 carboxylate (i.e., $GA_{15}$) is presumably due to the presence of the δ-lactone ring. However, no peak exhibiting the expected molecular mass and/or retention time for $GA_9$-aldehyde was observed.

GA biosynthetic intermediates prior to $GA_{12}$-aldehyde do not have the characteristic gibberellane 6-5-6-5 ring structure, but instead a 6-6-6-5 *ent*-kaurane ring structure. While addition of the olefin precursor *ent*-kaurene to *Et*CYP112 only induces a small shift of the Soret-band, with no decrease in α-band absorption, surprisingly, the oxygenated derivatives

induced typical type I binding spectra. In particular, *ent*-kaurenoic acid, its methylated derivative (methyl *ent*-kaurenoate), *ent*-7α-hydroxy kaurenoic acid, *ent*-kaurenal and *ent*-kaurenol, for which the $K_d$ values were calculated to be 2.7, 0.5, 3.4, 18 and 27 μM, respectively (Table 1 and Figures 6 and S4). However, no products were observed from assays with these compounds (data not shown).

## Discussion

The substrate specificity of the *E. tracheiphila* CYP112 isozyme was tested here. This was enabled by its ready over-expression in *E. coli*, perhaps reflecting their relatively close phylogenetic relationship (i.e., both species fall within the Enterobacteriaceae family). However, unlike *Et*CYP117, which catalyzes the first oxidative transformation in the GA biosynthetic pathway (Figure 1) and also is readily over-expressed in *E. coli* (14), *Et*CYP112 can be purified with retention of catalytic activity and exhibits the characteristic Soret-band at about 420 nm, as well as the characteristic Soret peak at 450 nm after reduction and CO binding.

Based on the ability to measure binding with straightforward UV-Vis spectral studies it was possible to examine the affinity of *Et*CYP112 for a number of GA biosynthetic intermediates, as well as selected methylated derivatives (Table 1). In contrast to at least a GA20ox from wheat (*Triticum aestivum*) that exhibited increased $K_M$ values for the catalyzed reaction intermediates $GA_{15}$ (open) and $GA_{24}$ relative to $GA_{12}$ (15), *Et*CYP12 exhibits decreased $K_d$ (i.e., higher affinity) for these. This is consistent with their observed retention in the active site during the course of the catalyzed series of reactions (9). While the $K_M$ values for GA20ox and $K_d$ values for *Et*CYP112 cannot be directly compared, they are both in the upper nM to lower μM range (no binding affinities have been reported for the fungal equivalent CYP68B). Given the highly bioactive nature of GAs low production levels are sufficient to induce an effect, consistent with the tight binding observed here. In addition to $GA_{12}$, $GA_{15}$ and $GA_{24}$, *Et*CYP112 was found to bind, at least to some degree, essentially all precursors in the bacterial GA biosynthetic pathway, as well as the methylated derivatives of its substrates and reaction intermediates. Surprisingly, this included precursors with the 6-6-6-5 *ent*-kaurane rather than 6-5-6-5 gibberellane ring structure. Although *ent*-kaurene and its derivatives did not serve as substrates, some spectral change was observed in Soret-band absorption upon their addition to *Et*CYP112. Accordingly, these precursors can bind and displace the water molecule that coordinates the heme-Fe(III) as its sixth ligand, leading to some conversion to the spectrally observed high-spin state. However, unlike the native reactants, these precursors do not fully convert *Et*CYP112 to the high-spin state (i.e., this is generally below <60%). This promiscuous binding may be linked to the complex reactions catalyzed by *Et*CYP112, as these involve relatively large changes in the structure of the reactant. Nonetheless, *Et*CYP112 exhibits higher fidelity in terms of activity, since only the natural substrate and intermediates are efficiently reacted upon. Indeed, even the immediate precursor $GA_{12}$-aldehyde, which particularly in its *geminal*-diol form is a close structural analog of $GA_{12}$, is not efficiently acted upon by *Et*CYP112. Accordingly, the different ring structure of *ent*-kaurene and its derivatives must alter their positioning in the *Et*CYP112 active site such that they are not correctly oriented for catalysis (i.e., relative to the thiolate

heme-iron), despite their ability to (partially) displace the water molecule otherwise serving as the 6th ligand.

It was previously shown that *Et*CYP112 does not react with either the C-20 carboxylate $GA_{25}$ or the 7,19-dimethyl ester derivative of $MeGA_{24}$ (9). Here this was found to be at least partially due to the fact that neither compound binds to *Et*CYP112 with a significant shift of the Soret-band and decrease of the α-band. Together these findings support the previously indicated use of a cyclic anhydride C-20 *gem*-diol intermediate, as methylation of the C-19 carboxylate in $MeGA_{24}$ prevents cyclization and $GA_{25,}$ while theoretically able to cyclize to the anhydride, is energetically unlikely do so in an aqueous environment.

In conclusion, the studies reported here provide insight into the impact of the complex transformation of $GA_{12}$ to $GA_9$ on the substrate structure-function relationship of CYP112, which must accommodate significant changes in its substrate/reactants (see Figure 1B). This is shown to be reflected, in promiscuous binding of upstream precursors. Nevertheless, although these preceding metabolites can bind to CYP112, they only do so with a higher $K_d$ or a reduced ability to convert the thiolate heme-iron to its high-spin state. Accordingly, CYP112 reactivity seems to be quite specific. Of the various biosynthetic precursors bound by CYP112, only $GA_{12}$-aldehyde is reacted upon, and even this is only slowly and partially transformed, with no catalysis of the final combined demethylation and γ-lactone ring forming reaction. This presumably is a function of the complexity of this final transformation (i.e., from $GA_{24}$ to $GA_9$), and corresponding requirement for precise positioning of the substrate/reactant within the active site. Regardless, these results indicate that, despite the need to accommodate significant alteration of its substrate/reactants during transformation of $GA_{12}$ to $GA_9$, leading to promiscuous binding of upstream metabolites, CYP112 only readily reacts with its natural substrate and reaction intermediates. Accordingly, the role of CYP112 in bacterial GA biosynthesis is specified at the catalytic rather than substrate binding level.

## Supplementary Material

Refer to Web version on PubMed Central for supplementary material.

## Acknowledgments

We wish to thank ISU Chemical Instrumentation Facility staff member Steve Veysey for assistance with the Waters GCT GC-MS analyses, and Prof. Peter Hedden (Rothamsted Research) for $GA_{12}$ and $GA_{25}$ standards.

**Funding**

This work was supported by grants from the NIH (GM109773) and NSF (CHE-1609917) to R.J.P., along with a postdoctoral fellowship to R.N. from the Deutsche Forschungsgemeinschaft (DFG) NA 1261/1-2.

## Abbreviations List

| | |
|---|---|
| **GA** | Gibberellin |
| **CYP** | cytochrome P450 |
| **2ODD** | 2-oxoglutarate dependent dioxygenases |

| | |
|---|---|
| **GA20ox** | GA 20-oxidase |
| ***Et*CYP112** | *Erwinia tracheiphila* CYP112 |
| ***Et*FdR** | *E. tracheiphila* ferredoxin reductase |
| ***Et*SDR** | *E. tracheiphila* short-chain alcohol dehydrogenase/reductase |
| **GC-MS** | gas chromatography mass spectrometry |

## References


1. Hedden P, Sponsel V. A Century of Gibberellin Research. J Plant Growth Regul. 2015; 34(4):740–60. [PubMed: 26523085]
2. Nagel R, Peters RJ. Investigating the Phylogenetic Range of Gibberellin Biosynthesis in Bacteria. Molecular Plant-Microbe Interactions. 2017; 30(4):343–9. [PubMed: 28425831]
3. Nagel R, Turrini PC, Nett RS, Leach JE, Verdier V, Van Sluys MA, et al. An operon for production of bioactive gibberellin A4 phytohormone with wide distribution in the bacterial rice leaf streak pathogen *Xanthomonas oryzae* pv. *oryzicola*. New Phytologist. 2017; 214(3):1260–6. [PubMed: 28134995]
4. Nett RS, Montanares M, Marcassa A, Lu X, Nagel R, Charles TC, et al. Elucidation of gibberellin biosynthesis in bacteria reveals convergent evolution. Nature Chemical Biology. 2017; 13(1):69–74. [PubMed: 27842068]
5. Kamiya Y, Takahashi N, Graebe JE. The loss of carbon-20 in C19-gibberellin biosynthesis in a cell-free system from *Pisum sativum* L. Planta. 1986; 169(4):524–8. [PubMed: 24232760]
6. Ward JL, Gaskin P, Brown RGS, Jackson GS, Hedden P, Phillips AL, et al. Probing the mechanism of loss of carbon-20 in gibberellin biosynthesis. Synthesis of gibberellin 3α,20-hemiacetal and 19,20-lactol analogues and their metabolism by a recombinant GA 20-oxidase. Journal of the Chemical Society, Perkin Transactions 1. 2002; (2):232–41.
7. Ward JL, Jackson GJ, Beale MH, Gaskin P, Hedden P, Mander LN, et al. Stereochemistry of the oxidation of gibberellin 20-alcohols, $GA_{15}$ and $GA_{44}$, to 20-aldehydes by gibberellin 20-oxidases. Chemical Communications. 1997; (1):13–4.
8. Dockerill B, Hanson JR. The fate of C-20 in C19 gibberellin biosynthesis. Phytochemistry. 1978; 17(4):701–4.
9. Nagel R, Peters RJ. Diverging Mechanisms: Cytochrome-P450-Catalyzed Demethylation and gamma-Lactone Formation in Bacterial Gibberellin Biosynthesis. Angew Chem Int Ed Engl. 2018; 57(21):6082–5. [PubMed: 29517843]
10. McLean KJ, Warman AJ, Seward HE, Marshall KR, Girvan HM, Cheesman MR, et al. Biophysical characterization of the sterol demethylase P450 from *Mycobacterium tuberculosis*, its cognate ferredoxin, and their interactions. Biochemistry. 2006; 45(27):8427–43. [PubMed: 16819841]
11. Tudzynski B, Rojas MC, Gaskin P, Hedden P. The gibberellin 20-oxidase of *Gibberella fujikuroi* is a multifunctional monooxygenase. J Biol Chem. 2002; 277(24):21246–53. [PubMed: 11943776]
12. Bearder JR, MacMillan J, Phinney BO. Fungal products. Part XIV. Metabolic pathways from *ent*-kaurenoic acid to the fungal gibberellins in mutant B1-41a of *Gibberella fujikuroi*. Journal of the Chemical Society, Perkin Transactions 1. 1975; (8):721–6.
13. Gaskin, P., MacMillan, J. GC-MS of the gibberellins and related compounds : methodology and a library of spectra. Bristol: Univ. of Bristol (Cantocks Enterprises Ltd); 1991.
14. Nagel R, Peters RJ. $^{18}O_2$ labeling experiments illuminate the oxidation of *ent*-kaurene in bacterial gibberellin biosynthesis. Organic & Biomolecular Chemistry. 2017; 15(36):7566–71. [PubMed: 28858359]
15. Appleford NEJ, Evans DJ, Lenton JR, Gaskin P, Croker SJ, Devos KM, et al. Function and transcript analysis of gibberellin-biosynthetic enzymes in wheat. Planta. 2006; 223(3):568–82. [PubMed: 16160850]

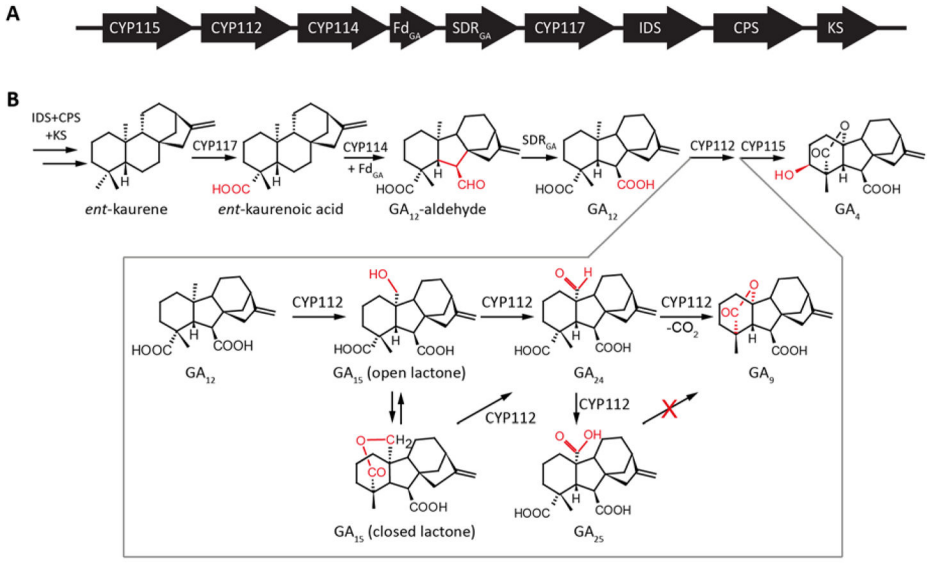


**Figure 1.**

Bacterial gibberellin operon (**A**) Schematic representation of the GA biosynthetic operon. Arrows indicate the direction of translation, abbreviations for the genes are CYP, cytochrome P450; Fd, ferredoxin; SDR, short-chain alcohol dehydrogenase/reductase; IDS, isoprenyl diphosphate synthase; CPS, copalyl diphosphate synthase; KS, *ent*-kaurene synthase; and IDI, isopentenyl diphosphate isomerase. (B) Catalyzed reactions, with emphasize on the sequential oxidation and elimination of C-20 from $GA_{12}$, to produce $GA_9$, by CYP112.

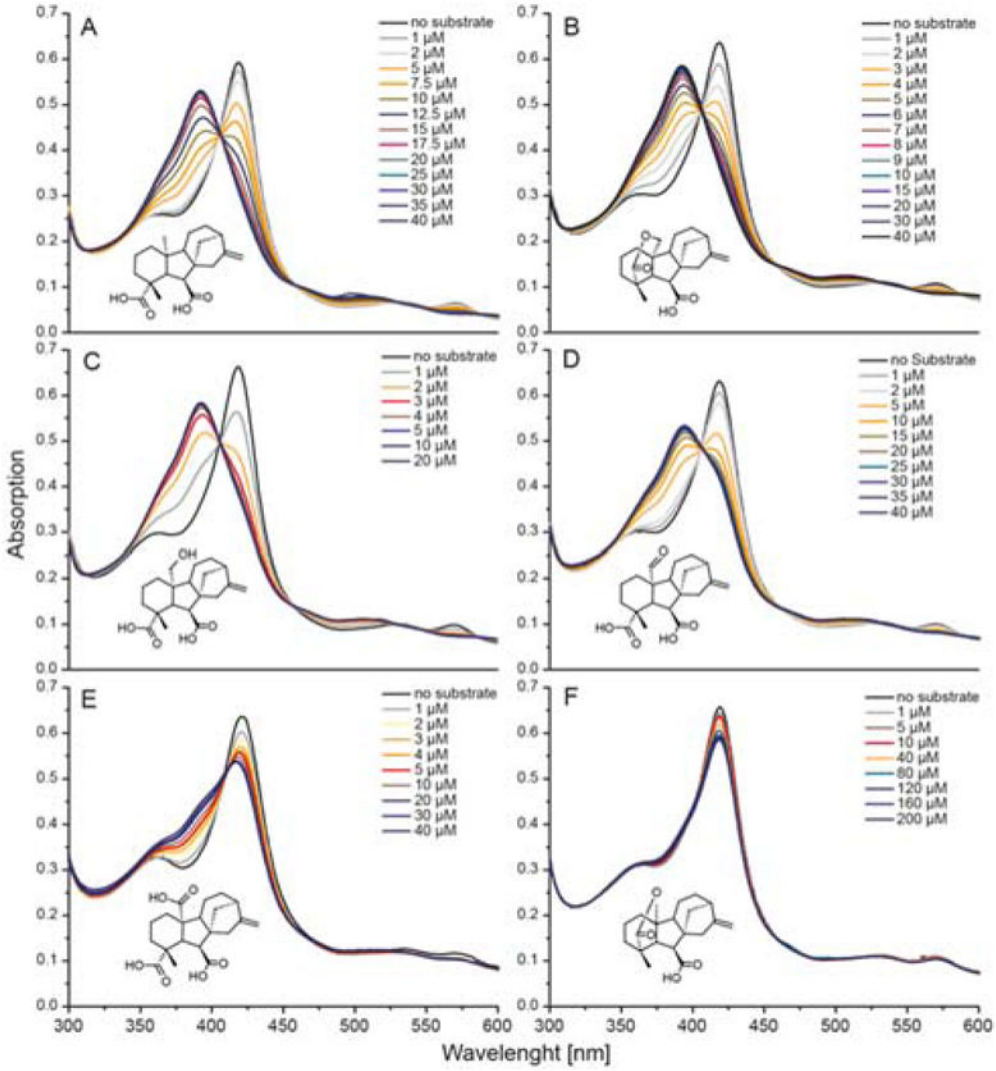


**Figure 2.**

Spectral titration of *Et*CYP112 with substrates and products. UV-Vis spectra of *Et*CYP112 in the absence and with increasing concentrations of (A) $GA_{12}$, (B) $GA_{15}$ (closed lactone), (C) $GA_{15}$ (open lactone), (D) $GA_{24}$, (E) $GA_{25}$ and (F) $GA_9$.

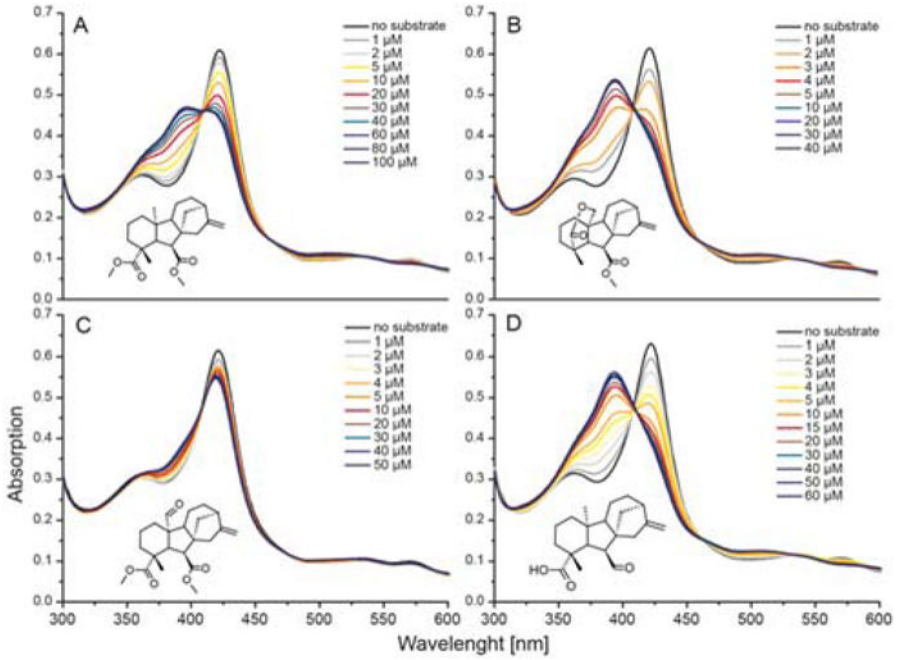


**Figure 3.**

Spectral titration of *Et*CYP112 with methylated substrates, as well as immediate precursor $GA_{12}$-aldehyde. UV-Vis spectra of *Et*CYP112 in the absence and with increasing concentrations of (A) $MeGA_{12}$, (B) $MeGA_{15}$ (closed lactone), (C) $MeGA_{24}$ and (D) $GA_{12}$-aldehyde.

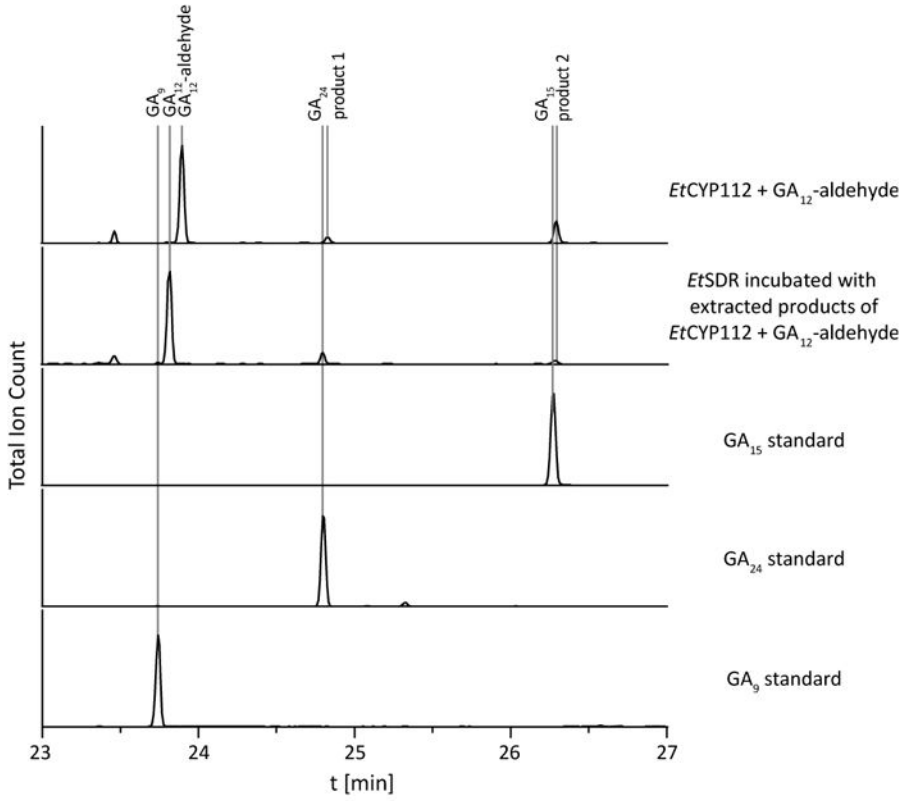


**Figure 4.**

Conversion of $GA_{12}$-aldehyde by *Et*CYP112. GC-MS-chromatograms of *in vitro* assays with *Et*CYP112 and $GA_{12}$-aldehyde, incubation of the products with *Et*SDR and $GA_{15}$, $GA_{24}$ and $GA_9$ standards.

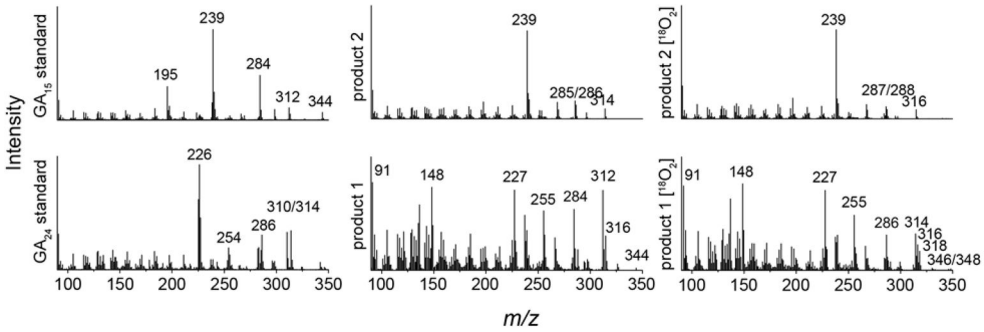


**Figure 5.**

Mass spectra of $GA_{15}$- and $GA_{24}$-aldehyde. MS spectra of standard compounds and the unknown products of enzyme assays with *Et*CYP112 and $GA_{12}$-aldehyde, either under regular atmosphere or $^{18}O_2$. Presented mass spectra were acquired with a Varian 2100T ion trap mass spectrometer.

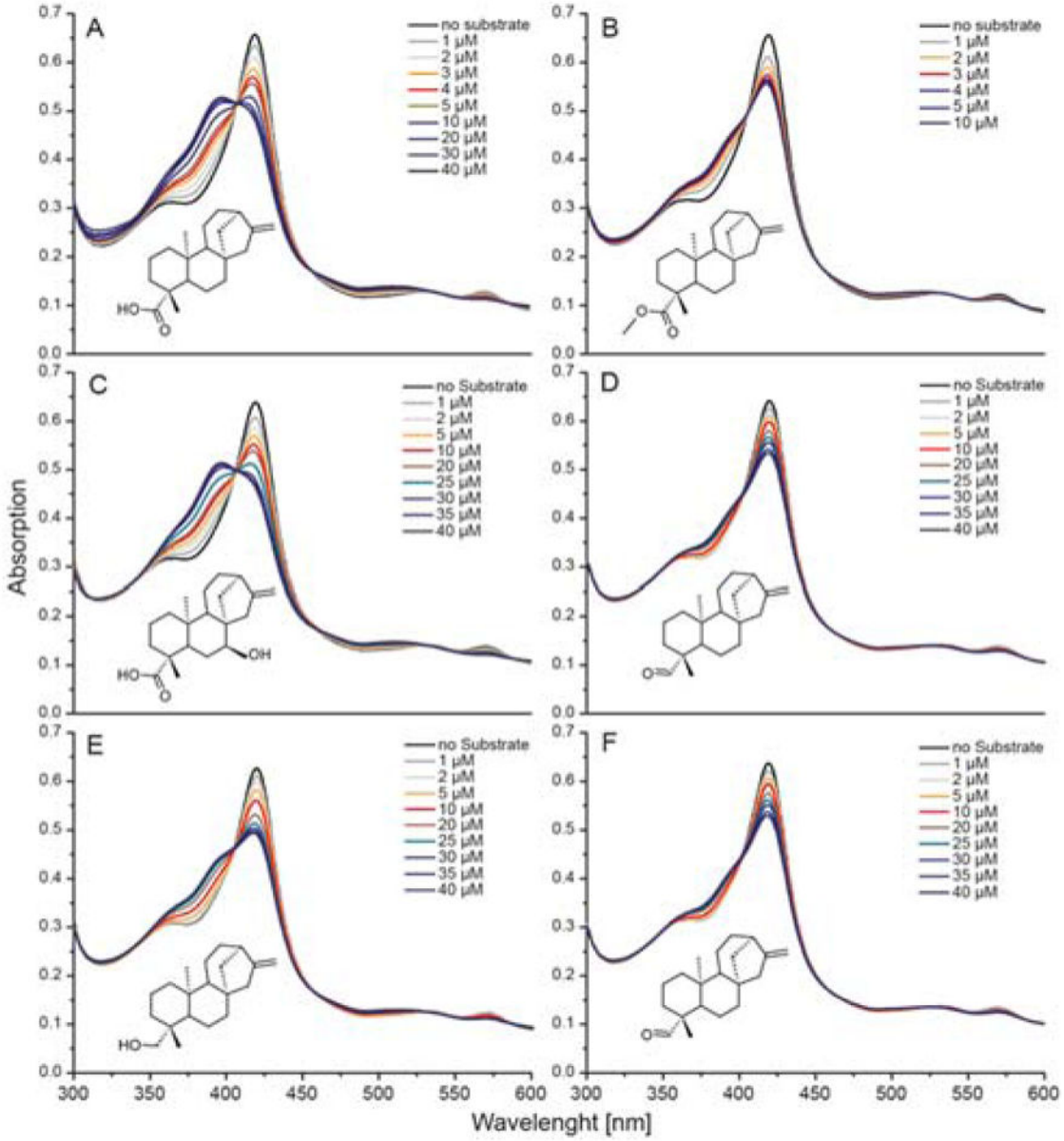


**Figure 6.**

Spectral titration of *Et*CYP112 with kaurane precursors. UV-Vis spectra of *Et*CYP112 in the absence and with increasing concentrations of (A) *ent*-kaurenoic acid, (B) methyl *ent*-kaurenoate, (C) *ent*-7α-hydroxy-kaurenoic acid, (D) *ent*-kaurenal, (E) *ent*-kaurenol, and (F) *ent*-kaurene.

## Table 1

*Et* CYP112 affinity for GA metabolites and methylated derivatives.

| Substrate | $K_d$ [μM] | High Spin State | α-band Absorbtion |
|---|---|---|---|
| $GA_{12}$ | 2.6 ± 0.3 | > 90% | decreased |
| $GA_{15}$ (open lactone) | 0.11 ± 0.02 | > 90% | decreased |
| $GA_{15}$ (closed lactone) | 0.6 ± 0.1 | > 90% | decreased |
| $GA_{24}$ | 0.32 ± 0.07 | 80 – 90% | decreased |
| $GA_9$ | n.a. | < 5% | ***unchanged*** |
| $GA_{25}$ | n.a. | 10 – 20% | ***unchanged*** |
| $GA_{12}$-aldehyde | 2.0 ± 0.3 | > 90% | decreased |
| $MeGA_{12}$ | 14 ± 3 | 50 – 60% | decreased |
| $MeGA_{15}$ | 0.11 ± 0.03 | 80 – 90% | decreased |
| $MeGA_{24}$ | n.a. | 5 – 10% | ***unchanged*** |
| *ent*-kaurenoic acid | 2.7 ± 0.6 | 50 – 60% | decreased |
| methyl-*ent*-kaurenoate | 0.5 ± 0.1 | 10 – 15% | decreased |
| *ent*-7α-hydroxy kaurenoic acid | 3.4 ± 0.6 | 50 – 60% | decreased |
| *ent*-kaurenal | 18 ± 2 | 5 – 10% | decreased |
| *ent*-kaurenol | 27 ± 7 | 20 – 30% | decreased |
| *ent*-kaurene | n.a. | < 5% | ***unchanged*** |

The $K_d$ and the standard error were calculated from 3 independently performed titration experiments.